

Manipulation of Nonlinear Optical Properties of Graphene Bonded Fiber Devices by Thermally Engineering Fermi–Dirac Distribution

Cheng Li, Jin-hui Chen, Wan-sheng Wang, Tian-xing Wang, Shao-cheng Yan, Dan-ran Li, Fei Xu,* Cheng-bo Mou,* and Yan-qing Lu*

Graphene's atomic thickness, gapless Dirac–Fermionic band structure, and large thermal conductivity make it a promising element for applications in photonic integrated devices. Importantly, actively tunable graphene-waveguide-integrated optoelectronic devices can potentially be utilized for the realization of reconfigurable photonic systems. Since electrical device control is always preferred, researchers have previously demonstrated gate-variable graphene devices; however, electrical control remains challenging, particularly in all-fiber systems because of the required complicated configuration and fabrication techniques along with additional signal loss. Here, a graphene-fiber-integrated platform is proposed and the manipulation of its nonlinear optical properties is demonstrated by engineering the Fermi–Dirac distribution of graphene based on a convenient electric heating method. For the first time, it is experimentally shown that the nonlinear optical absorption of graphene is correlated to temperature via the thermal relaxation process. In the experiments, the modulation depth variation exceeds 60%. The configuration is simple, cost-effective, and can be readily extended to other 2D materials. It is believed that this work can contribute to building miniature and compact graphene-fiber-integrated devices for actively tunable multifunctional applications.

silica-fiber-based optoelectronics devices, circuits, and systems.^[1–4] A number of advanced graphene-based photonic applications have been proposed and demonstrated, including optical modulators, photodetectors, polarizers, mode-locked lasers, and sensors.^[5–9] One of the exciting prospective features of graphene devices is the capability of active manipulation of its properties.^[10–12] A number of techniques have been developed to manipulate graphene's electronic, mechanical, and optical properties, ranging from chemical doping and strain engineering to electric gating. Among these, actively controllable photonic devices realized via electrically changing the Fermi level exhibit fascinating flexibility. For example, tunable optical modulators have been demonstrated via electrical gating of single graphene layer integrated with silicon waveguides or photonic crystal nanocavities.^[6,13,14] Along with these lines, in fiber systems, researchers have recently

Graphene, which is an allotrope of carbon in the form of a 2D atomic-scale, hexagonal lattice, has attracted intense attention because of its atomic thickness and unique fundamental physical properties, particularly in the context of applications in next-generation on-chip planar silicon waveguides or

reported an electrically tunable inline graphene device that integrates graphene-based field effect transistors with ionic liquid on a side-polished fiber.^[15] However, such conventional electronic operations on the Fermi level through gating configurations require complicated fabrication techniques, which are particularly challenging to realize in all-fiber systems. Meanwhile, the optical conductivity of graphene has theoretically been shown to be related to not only the Fermi level but also the temperature.^[16,17] Consequently, the active manipulation of graphene devices can also be realized through thermal engineering and the thermal modulation of graphene devices at linear optics range is demonstrated,^[18,19] nevertheless, the nonlinear absorption of graphene with thermal tuning has not thus far been experimentally realized.

In this work, for the first time, we successfully demonstrate the active manipulation of the nonlinear optical properties of a graphene-fiber-integrated device (GFD) by electrically varying the temperature. The GFD is fabricated by directly bonding multilayer graphene onto a fiber facet to act as a nanoheater. By tuning the applied electrical current from 0 to 9 mA, the temperature of graphene can be alternated between ≈ 300 and ≈ 900 K (see Figure S1 in the Supporting Information), which in turn modifies graphene's optical conductivity. Hence, the

Dr. C. Li, J.-H. Chen, S.-C. Yan, D.-R. Li, Prof. F. Xu, Prof. Y.-Q. Lu
National Laboratory of Solid State Microstructures
College of Engineering and Applied Sciences and Collaborative
Innovation Center of Advanced Microstructures
Nanjing University
Nanjing 210093, P. R. China
E-mail: feixu@nju.edu.cn; yqlu@nju.edu.cn

Prof. W.-S. Wang
Department of Physics
Ningbo University
Ningbo 315211, P. R. China

T.-X. Wang, Prof. C.-B. Mou
Key Laboratory of Specialty Fiber Optics and Optical Access Networks
Shanghai University
Shanghai 200072, P. R. China
E-mail: mouc1@shu.edu.cn

 The ORCID identification number(s) for the author(s) of this article can be found under <https://doi.org/10.1002/adom.201700630>.

DOI: 10.1002/adom.201700630

nonlinear optical absorption (saturable absorption, SA) can be modified by tuning the thermal temperature. As a result, the modulation depth of graphene SA varied from 2.3 to 0.9%, with a total variation exceeding 60%, which is consistent with the theoretical calculation. Finally, we incorporate the optical modulator into a fiber laser circuit to demonstrate the fiber laser's operation state (mode-locked or continuous-wave) and pulse width (see Figure S3 in the Supporting Information), which can be tuned by the electrical current. Our configuration is simple, cost-effective, and can be readily extended to other 2D materials. We believe that our approach can lead to the fabrication of miniature, compact and practical GFDs for actively tunable multifunctional applications.

Figure 1a shows the schematic of a GFD device. The GFD is fabricated by transferring multilayer graphene onto a fiber end-face with a pair of gold electrodes (see the Experimental Section). The inset in Figure 1a shows the microscopic image of the GFD and the SEM image of graphene. The gap between the electrodes is about 20 μm . The graphene acts as a nanoheater that can control its temperature. Figure 1b shows the measured Raman spectra of the graphene before applying current; the G mode is at 1591.8 cm^{-1} .

The heating power P_{heating} of this nanoheater is related to the electric current and resistance as follows^[20]

$$P_{\text{heating}} = I^2 R_{\text{FG}} \quad (1)$$

The resistance of GFD includes two components: the resistance of the graphene sheets between the electrodes, R_G , and the contact resistance between the gold film and graphene, R_{Con} ^[21]

$$R_{\text{FG}} = R_G + R_{\text{Con}} = R_s L/w + 2R_c/w \quad (2)$$

Here, R_s denotes the sheet resistance of graphene, R_c is the contact resistivity between the graphene and gold layers, L is the length of graphene between the electrodes, and w indicates the width of the contact part. To obtain the values of R_s and R_c , we measured the resistance of the GFD for different lengths L . By fitting the results, we obtained the R_s and R_c values from Equation (2) as shown in Figure 1c. According to the result of linear fit, the $R_s \approx 2000 \Omega$ and $R_c \approx 1000 \Omega \mu\text{m}$. Further, L equals the length of the gap between electrodes, 20 μm , and w equals the diameter of the fiber, 125 μm . Thus, the total resistance of

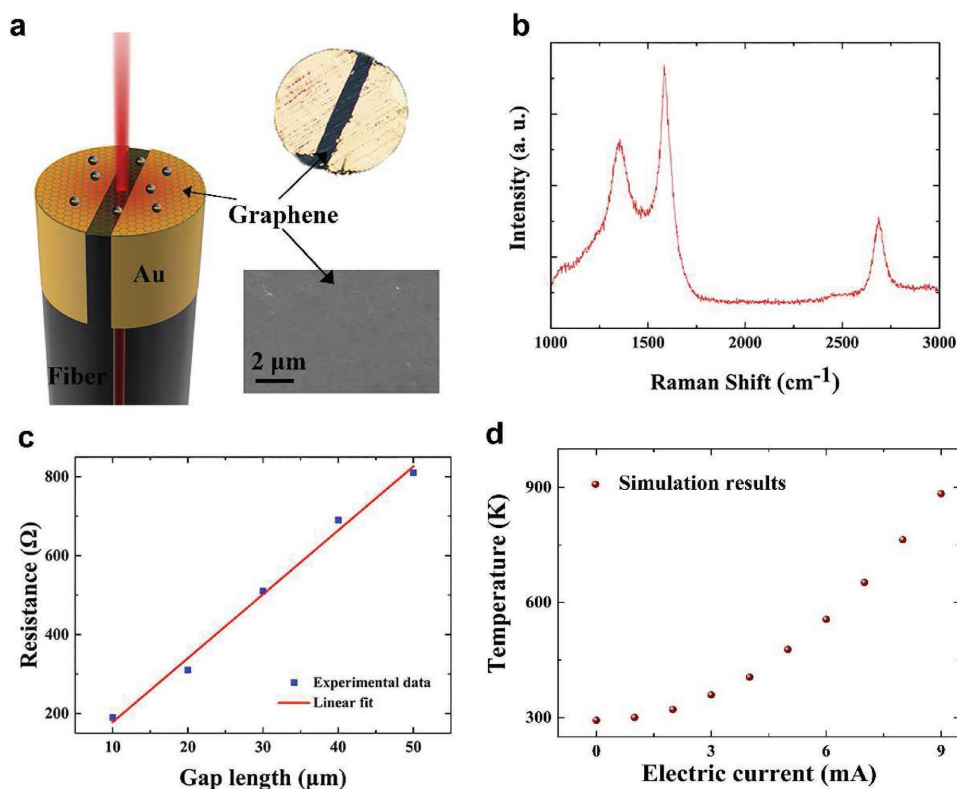


Figure 1. Schematic and image of graphene-fiber-integrated device (GFD) and its characteristics. a) Schematic description of GFD. The GFD is fabricated by transferring graphene onto a fiber end-face with a pair of gold electrodes. Lapping films and a tapered tungsten needle are used to remove the gold in the mid-section to form the gap. Upper right part of panel (a) shows the microscopic image of the GFD. The thickness of the gold film is about 100 nm, which makes it easy to remove the gold film while ensuring good electrical conductivity. The gap between the gold electrodes is about 20 μm . Lower right part of panel (a) is the SEM image of the graphene, it shows the graphene has good uniformity. b) The Raman spectra of graphene at $I = 0$ mA, the G mode at 1591.8 cm^{-1} . c) The resistances of GFD as the function of gap length. The resistances of the graphene with different gap length are measured. Through the linear fit, $R_s \approx 2000 \Omega$ and $R_c \approx 1000 \Omega \mu\text{m}$. d) Temperature characteristic of GFD as a function of injected electric current. The temperature elevates with increasing electric current. At 9 mA, the temperature is around 900 K, which is close to the melting point of gold. Thus, the GFD acts as a high-performance nanoheater.

the GFD is about 336 Ω , whose value is in agreement with the measured experimental result ($\approx 300 \Omega$).

Upon tuning the electric current from 0 to 9 mA, the heating power increases from 0 to 24.3 mW. In our study, the temperature of the graphene section was simulated with the COMSOL package based on the abovementioned data, and Figure 1b shows the simulation results. The temperature is around 900 K when the current is 9 mA, which means that the GFD can achieve high temperatures under low heating powers.

The Fermi–Dirac distribution can be expressed as

$$f_d(E) = \frac{1}{e^{(E-E_f)/k_B T} + 1} \quad (3)$$

Where E_f represents the Fermi level, k_B denotes the Boltzmann constant, and T is the electron temperature.

The optical conductivity of graphene depends on the Fermi–Dirac distribution, and in this regard, certain theories and experiments focusing on changing the optical properties of graphene via tuning the Fermi level have been reported.^[11,15] However, the configurations are often complex in addition to inducing high loss to the system.^[22] Moreover, the SA variation is irregular and inconsistent.

On the other hand, Equation (3) manifests the possibility of thermally tuned Fermi–Dirac distribution. The GFD, with its simple structure and inherent low loss, can be easily subjected to temperature changes via injection of electric current.

Figure 2 depicts the current-dependent SA of our GFD (see the Experimental Section, and Figure S4 in the Supporting Information). The optical loss of GFD is 14.6%. The loss of GFD includes two contributions: the absorption of graphene and the insertion loss of device. The typical insertion loss of our sample is 0.2 dB (4.5%). So the absorption of graphene is 10.1%. Considering the typical absorption of graphene is 2.3% per layer,^[23] the layer number of our graphene is about four layers. When the electrical current is absent, the modulation depth of the GFD is 2.3%, as shown in Figure 2a. In Figure 2b, with the current increase to 5.5 mA, the optical transmittance of the GFD at low peak intensity markedly increases, while the high-intensity transmittance changes by very little due to saturation effect. Figure 2c,d shows the transmittance under currents of 8.5 and 9 mA, respectively. We note that the transmittance for both cases exhibits similar behavior of further reduced modulation depth compared to that in Figure 2b. When $I = 9$ mA, the modulation depth of the GFD is 0.9%. We notice that if the current is 10 mA, the corresponding temperature will be too high; the graphene nanoheater cannot continue to function. However, such high temperature is close to the melting point of gold and the oxidizing temperature of graphene which is higher than 600°C for 3–5 layers graphene (see Figure S1 in the Supporting Information),^[24] the high temperature would degrade the performance of device. Therefore, in our study, the current was restricted to 10 mA to prevent the high temperature-induced GFD damage. The overall modulation depth

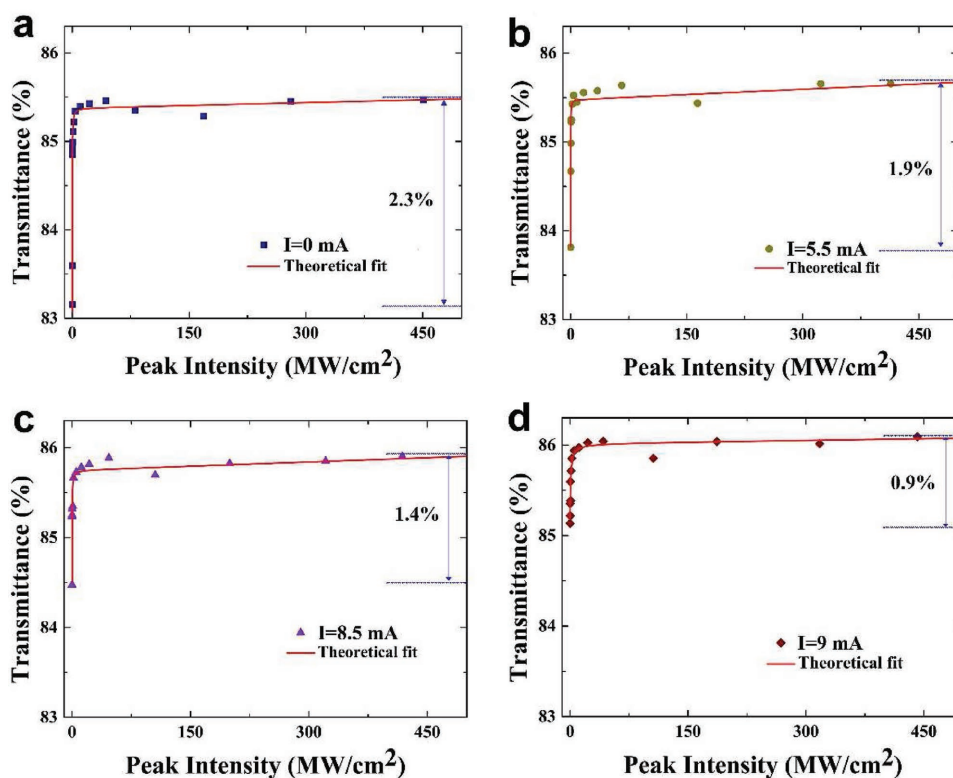


Figure 2. Nonlinear optical properties of graphene at different currents. Saturable absorption (SA) measurement of our graphene-fiber-integrated device (GFD) for different light intensities at a) $I = 0$ mA (transmittance change from 83.1 to 85.4%, modulation depth of 2.3%), b) $I = 5.5$ mA (transmittance change from 83.8 to 85.7%, modulation depth of 1.9%), c) $I = 8.5$ mA (transmittance change from 84.5 to 85.9%, modulation depth of 1.4%), and d) $I = 9$ mA (transmittance change from 85.1 to 86.0%, modulation depth is 0.9%). The threshold intensity is 1 MW cm⁻².

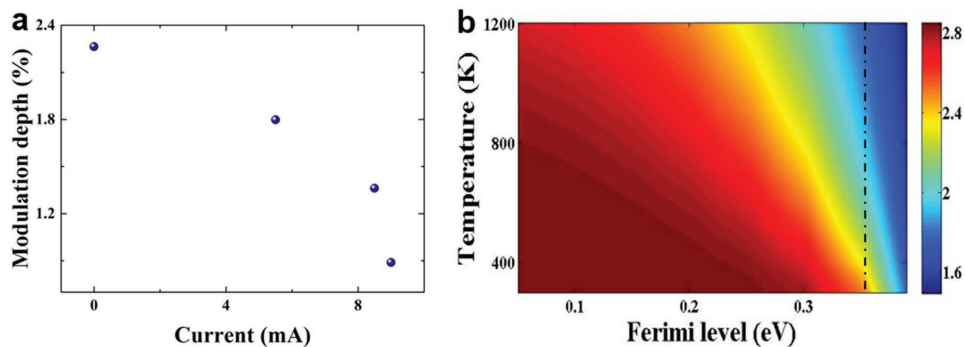


Figure 3. Experimental results and numerical calculations of modulation depth of graphene. a) The measured modulation depth of graphene under different electric current values. The modulation depth varies from 2.3 to 0.9%, and the variation exceeds 60%. b) The calculated modulation depth of graphene at different Fermi levels and temperatures. The modulation depth decreases with increase in the Fermi level and temperature. The dashed line indicates the modulation depth change from 2.5 to 1.76% when the Fermi level is 0.35 eV. This calculation is similar to our experimental result, which means that the Fermi level of our graphene-layer section is ≈ 0.35 eV.

variation from 2.3 to 0.9%, is illustrated in **Figure 3a**. It can be seen that the modulation depth monotonically changes against the electric current with a total variation of over 60%.

To validate our experimental results, we simulated the optical property of graphene at different temperatures. Because the modulation depth is considerably higher for interband absorption than intraband absorption, only the interband SA will be considered during our simulation. The absorption of graphene can be expressed as^[25]

$$\alpha_{\text{inter}} \equiv \frac{\int_{-\pi/\omega}^{+\pi/\omega} \mathbf{J}_{\text{inter}}(t) \cdot \mathbf{E}(t) dt}{(2\pi/\omega)I_0} \quad (4)$$

Here, $\mathbf{E}(t)$ represents the optical field, ω is the angular frequency, I_0 is the peak intensity, and $\mathbf{J}_{\text{inter}}(t)$ denotes the interband current density, which can be derived via a nonperturbative approach. Next, we numerically solved Equation (4) to obtain the relationship between the graphene modulation depth and the Fermi level and temperature, as shown in **Figure 3b**. From the figure, we note that the modulation depth decreases with increase in the Fermi level

and temperature. When the Fermi level equals 0.35 eV, the variation in the modulation depth is close to that observed in our experiment (dashed line in **Figure 3b**). The modulation depth changes from 2.5 to 1.76%.

To better understand the relationship between the injection current and the nonlinear optical property, we measured the transmittance at low (far below the threshold intensity of $\approx 1 \text{ MW cm}^{-2}$) and high peak intensities (far above the threshold intensity). **Figure 4a** (top panel) shows the change in transmittance at low peak intensity. With the current levitation from 0 to 9 mA, the transmittance rapidly increases from 83.1 to 85.1%. The total increase in the transmittance at low intensities is nearly 2%. When compared with the modulation depth at 0 mA (and the corresponding transmittance), this increase is significant. However, at high peak intensities, as shown in **Figure 4a** (bottom panel), the transmittance changes from 85.4 to 86.0%, which is an increase of merely 0.6%.

Figure 4b simulates the transmittance change at different temperatures at low (top panel) and high (bottom panel) peak intensities as per Equation (4) (with the Fermi level being equal to 0.35 eV), and we note that the results are similar to those in **Figure 4a**. The transmittance variation at low intensity is more

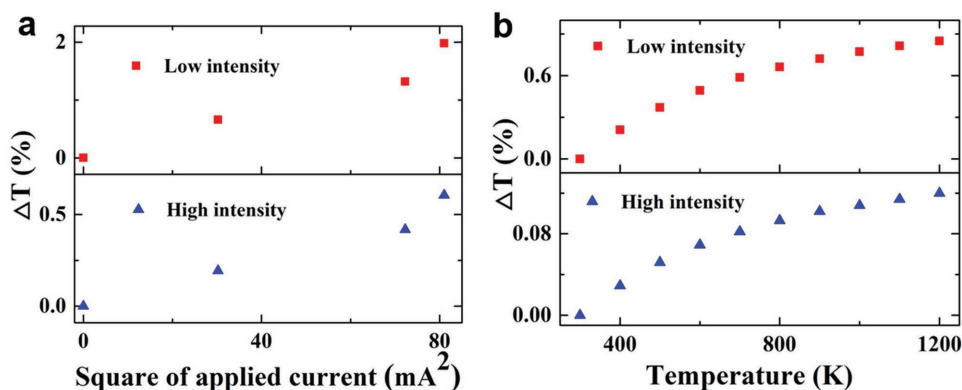


Figure 4. Relationship between transmittance and light intensity. a) Change in transmittance with increasing current (temperature) at low (top panel) and high peak intensities (bottom panel). With an increase in the electric current, the variation in the transmittance at low peak intensity is 3.3 times that at high intensity. b) Simulated variation in transmittance at low intensity (top panel) and high intensity (bottom panel) for a Fermi level of 0.35 eV. Obviously, the transmittance variation at low intensity is larger than that at high intensity, which is in agreement with our experimental results.

significant than that at high intensity when the temperature is varied. The small mismatch between the experiments and simulations is due to the ignorance of intraband SA and possible defects in graphene in simulation. The transmittance exhibits a significant difference between low and high peak irradiation intensities at different temperatures, indicating that graphene is an excellent nonlinear thermo-optic material.

The GFD, which can easily be integrated within a fiber system, allows continuous tuning of modulation depth with the injection of an electric current. Thus, our GFD can be used as a key device to manipulate the performance of a fiber laser. In our study, we constructed a typical fiber ring-cavity laser incorporating a modulation depth tunable SA based on GFD (Figure S2, Supporting Information).

Figure 5a–f shows the typical characteristics of a fiber laser based on the GFD at different currents. Figure 5a

shows the optical spectrum of the laser without applying current, while Figure 5b depicts the radio frequency spectrum of the laser. As regards laser operation, when the current is 0 mA, stable mode-locked pulses can be obtained, as shown in Figure 5c. The FWHM of the optical spectrum is about 0.61 nm, and the signal-to-noise ratio is over 75 dB. With increase in the current to 6 and 8 mA, the mode-locked pulses become unstable and weak, as shown in Figure 5d,e, respectively. With further increase in current to 9 mA, no stable mode-locked pulses are observed anymore, as shown in Figure 5f. Because the modulation depth changes with increase in the current, the conditions for the mode-locked fiber laser also vary. With increase in current, laser pulses are less likely to be formed. Thus, the current can be varied to obtain a switching fiber laser. Otherwise, the pulse width is related to the modulation depth of graphene, the

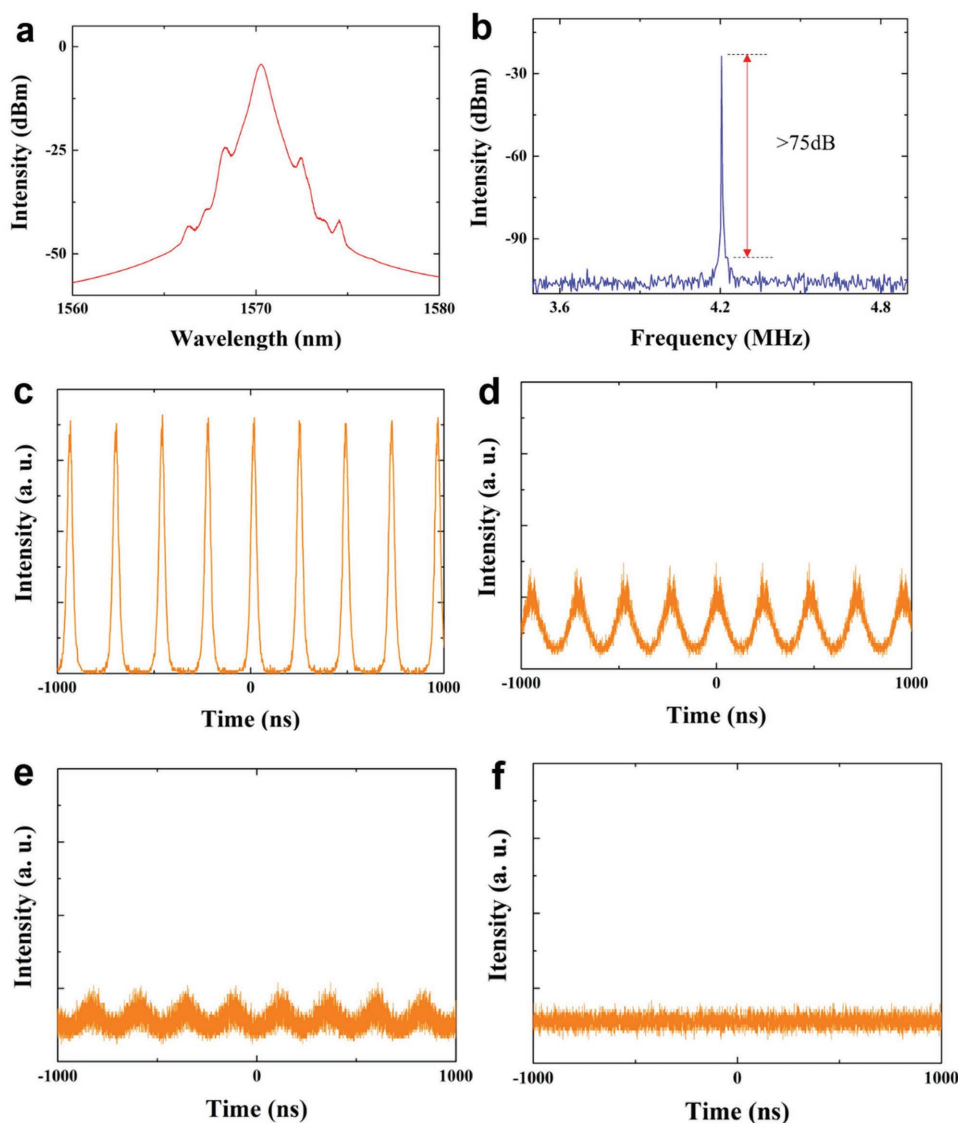


Figure 5. Versatile operation regime fiber laser based on graphene-fiber-integrated device. a) Spectrum of the fiber laser based on the GFD, and b) frequency spectrum of the laser. c) Stable mode-locked pulses obtained with a current of 0 mA. d),e) Laser outputs at currents of 6 and 8 mA, respectively. The pulses appear unstable and weak. f) The absence of pulses at a current of 9 mA.

dispersion of cavity and cavity birefringence. Figure 5 shows the pulses are unstable when the current is changed. But by simply adjusting the polarization controller, the stable mode-locked pulses can be obtained again (see Figure S3 in the Supporting Information).

In summary, for the first time to our knowledge, we have demonstrated the functioning of a temperature-tunable all-solid graphene-integrated fiber device with an extremely simple configuration. The fabrication of the device is simple, involving the direct bonding of a graphene sheets onto a fiber end-face. Via tuning the value of the applied current to the GFD from 0 to 9 mA, graphene can be heated over a range from ≈ 300 to ≈ 900 K according to our simulations. As a result, the nonlinear optical property of the GFD can be greatly modulated. Consequently, we successfully applied the GFD as a tunable nonlinear optical device in a fiber laser to realise a versatile mode-locked fiber laser. Our configuration is simple, cost-effective, and can be readily extended to other 2D materials. We believe that our study can contribute to the practical implementation of miniature and compact GFDs for actively versatile multifunctional applications.

Experimental Section

Fabrication of GFD: A cleaved and cleaned single-mode fiber (SMF-28, Corning) was coated with a gold film. The thickness of the gold film was about 100 nm, which made the gold suitably conductive while also facilitating its easy removal. Next, two layers of lapping films (LF1P, Thorlabs) were used to “scratch” the side of the fiber, and a tapered tungsten needle was employed to scratch the gold film on the fiber end-face, leaving behind a gap dividing the film into two sections. Next, a pair of electrodes was patterned on the fiber. Meanwhile, graphene (3–5 layers, ACS Materials) without a Cu substrate was prepared. Finally, the fiber was made to very lightly contact the graphene to transfer the graphene onto the fiber end-face.

Investigation of Saturable Absorption of GFD: The output of a commercial femtosecond fiber laser (C-Fiber HP, Menlo Systems) was connected to a fiber attenuator, and then split into two paths. One arm traveling through the GFD was detected by a high sensitivity optical power meter (PM100D, Thorlabs), while the power of the other beam was acquired by means of a reference power meter (model). An electric current source (2400 Source Meter, Keithley) was utilized to apply current to the GFD. After every increase/decrease in the current, several minutes were elapsed before the next trial in order to stabilize the device temperature.

Supporting Information

Supporting Information is available from the Wiley Online Library or from the author.

Acknowledgements

The authors acknowledge financial support from the National Natural Science Foundation of China (61535005 and 61475069) and National Science and Technology Major Projects (2017YFA0303700). The authors thank Prof. Xi-dong Xia, Prof. Xue-jin Zhang, and Fei Liu for their help with the experiments.

Conflict of Interest

The authors declare no conflict of interest.

Keywords

fiber lasers, graphene, temperature dependency

Received: June 30, 2017

Published online:

- [1] Q. Bao, K. P. Loh, *ACS Nano* **2012**, *6*, 3677.
- [2] F. Bonaccorso, Z. Sun, T. Hasan, A. C. Ferrari, *Nat. Photonics* **2010**, *4*, 611.
- [3] X. Wang, Z. Cheng, K. Xu, H. K. Tsang, J. B. Xu, *Nat. Photonics* **2013**, *7*, 888.
- [4] A. Martinez, Z. Sun, *Nat. Photonics* **2013**, *7*, 842.
- [5] F. Xia, T. Muller, Y. M. Lin, P. Avouris, *Nat. Nanotechnol.* **2009**, *4*, 839.
- [6] M. Liu, X. Yin, E. Ulin-Avila, B. Geng, T. Zentgraf, L. Ju, F. Wang, X. Zhang, *Nature* **2011**, *474*, 64.
- [7] J. T. Kim, C. G. Choi, *Opt. Express* **2012**, *20*, 3556.
- [8] Z. Sun, T. Hasan, F. Torrisi, D. Popa, G. Privitera, F. Wang, F. Bonaccorso, D. M. Basko, A. C. Ferrari, *ACS Nano* **2010**, *4*, 803.
- [9] G. S. Kulkarni, K. Reddy, Z. Zhong, X. Fan, *Nat. Commun.* **2014**, *5*, 4376.
- [10] A. Das, S. Pisana, B. Chakraborty, S. Piscanec, S. K. Saha, U. V. Waghmare, K. S. Novoselov, H. R. Krishnamurthy, A. K. Geim, A. C. Ferrari, A. K. Sood, *Nat. Nanotechnol.* **2008**, *3*, 210.
- [11] Z. Li, H. Qian, J. Wu, B. L. Gu, W. Duan, *Phys. Rev. Lett.* **2008**, *100*, 206802.
- [12] H. Xu, L. Xie, H. Zhang, J. Zhang, *ACS Nano* **2011**, *5*, 5338.
- [13] M. Liu, X. Yin, X. Zhang, *Nano Lett.* **2012**, *12*, 1482.
- [14] X. Gan, R. J. Shiue, Y. Gao, K. F. Mak, X. Yao, L. Li, A. Szep, D. Walker, J. Hone, T. F. Heinz, D. Englund, *Nano Lett.* **2012**, *13*, 691.
- [15] E. J. Lee, S. Y. Choi, H. Jeong, N. H. Park, W. Yim, M. H. Kim, J. K. Park, S. Son, S. Bae, S. J. Kim, K. Lee, Y. H. Ahn, K. J. Ahn, B. H. Hong, J. Y. Park, F. Rotermund, D. I. Yeom, *Nat. Commun.* **2015**, *6*, 6851.
- [16] G. W. Hanson, *J. Appl. Phys.* **2008**, *103*, 064302.
- [17] V. P. Gusynin, S. G. Sharapov, J. P. Carbotte, *J. Phys.-Condens. Mat.* **2007**, *19*, 249.
- [18] J. L. Benitez, J. Hernandez-coedero, S. Muhl, D. Mendoza, *Opt. Lett.* **2016**, *41*, 167.
- [19] S. Gan, C. Cheng, Y. Zhan, B. Huang, X. Gan, S. Li, S. Lin, X. Li, J. Zhao, H. Chen, Q. Bao, *Nanoscale* **2015**, *7*, 20249.
- [20] J. T. Smith, A. D. Franklin, D. B. Farmer, C. D. Dimitrakopoulos, *ACS Nano* **2013**, *7*, 3661.
- [21] L. Yu, Y. Yin, Y. Shi, D. Dai, S. He, *Optica* **2016**, *3*, 159.
- [22] Y. W. Song, S. Y. Jang, W. S. Han, M. K. Bae, *Appl. Phys. Lett.* **2010**, *96*, 051122.
- [23] R. R. Nair, P. Blake, A. N. Grigorenko, K. S. Novoselov, T. J. Booth, T. Stauber, N. M. R. Peres, A. K. Geim, *Science* **2008**, *320*, 1308.
- [24] L. Liu, S. Ryu, M. R. Tomasik, E. Stolyarova, N. Jung, M. S. Hybertsen, M. L. Steigerwald, E. L. Brus, G. W. Flynn, *Nano Lett.* **2008**, *8*, 1965.
- [25] A. Marini, J. D. Cox, F. J. G. De Abajo, *Phys. Rev. B* **2017**, *95*, 125408.